Earth and Space Science

RESEARCH ARTICLE
10.1029/2020EA001223

Termination of Solar Cycles and Correlated Tropospheric Variability

Robert J. Leamon[1,2], **Scott W. McIntosh**[3], **and Daniel R. Marsh**[3,4]

[1]Goddard Planetary Heliophysics Institute, University of Maryland-Baltimore County, Baltimore, MD, USA, [2]NASA Goddard Space Flight Center, Code 672, Greenbelt, MD, USA, [3]National Center for Atmospheric Research, High Altitude Observatory, Boulder, CO, USA, [4]Faculty of Engineering and Physical Sciences, University of Leeds, Leeds, UK

Abstract The Sun provides the energy required to sustain life on Earth and drive our planet's atmospheric circulation. However, establishing a solid physical connection between solar and tropospheric variability has posed a considerable challenge. The canon of solar variability is derived from the 400 years of observations that demonstrates the waxing and waning number of sunspots over an 11(-ish) year period. Recent research has demonstrated the significance of the underlying 22 years magnetic polarity cycle in establishing the shorter sunspot cycle. Integral to the manifestation of the latter is the spatiotemporal overlapping and migration of oppositely polarized magnetic bands. We demonstrate the impact of "terminators"—the end of Hale magnetic cycles—on the Sun's radiative output and particulate shielding of our atmosphere through the rapid global reconfiguration of solar magnetism. Using direct observation and proxies of solar activity going back some six decades we can, with high statistical significance, demonstrate a correlation between the occurrence of terminators and the largest swings of Earth's oceanic indices: the transition from El Niño to La Niña states of the central Pacific. This empirical relationship is a potential source of increased predictive skill for the understanding of El Niño climate variations, a high-stakes societal imperative given that El Niño impacts lives, property, and economic activity around the globe. A forecast of the Sun's global behavior places the next solar cycle termination in mid-2020; should a major oceanic swing follow, then the challenge becomes: when does correlation become causation and how does the process work?

Key Points:

- A solar cycle's fiducial clock does not run from the canonical min or max, instead resetting when all old cycle polarity flux is gone
- Observations over many solar cycles indicate that warm-to-cold transitions in the state of ENSO are correlated to the phase of this clock
- Cycle 24 is projected to end in mid-late 2020. Based on historical correlations, we anticipate a transition to La Niña at that time

Correspondence to:
R. J. Leamon,
robert.j.leamon@nasa.gov

Citation:
Leamon, R. J., McIntosh, S. W., & Marsh, D. R. (2021). Termination of solar cycles and correlated tropospheric variability. *Earth and Space Science*, *8*, e2020EA001223. https://doi.org/10.1029/2020EA001223

Received 10 APR 2020
Accepted 9 FEB 2021

Author Contributions:
Conceptualization: Robert J. Leamon, Scott W. McIntosh
Data curation: Robert J. Leamon, Scott W. McIntosh
Formal analysis: Robert J. Leamon, Scott W. McIntosh
Funding acquisition: Robert J. Leamon, Scott W. McIntosh
Investigation: Robert J. Leamon
Methodology: Robert J. Leamon
Validation: Robert J. Leamon, Scott W. McIntosh, Daniel R. Marsh
Visualization: Robert J. Leamon, Scott W. McIntosh
Scott W. McIntosh
Writing – original draft: Robert J. Leamon, Scott W. McIntosh, Daniel R. Marsh
Writing – review & editing: Robert J. Leamon, Scott W. McIntosh, Daniel R. Marsh

1. Introduction

Establishing a solid, physical, link between solar and tropospheric variability across timescales has posed a considerable challenge, despite the broad acknowledgment that the Sun provides the underlying energy to drive weather and climate (Gray et al., 2010). As it stands, solar connections to decadal-scale massive shifts in terrestrial weather patterns, like those of the North Atlantic Oscillation (NAO; Hurrell, 1995), or the El Nino Southern Oscillation (ENSO; Meehl et al., 2009) are little more than anecdotal. Investigations linking decadal-scale tropospheric activity with those of the Sun have relied on the canon of the 11 years solar activity cycle (Hathaway, 2015), requiring (apparently ad hoc) mathematical phase shifts to be introduced to establish *any* kind of link (Bal et al., 2011; Gray et al., 2010; van Loon et al., 2004; White & Liu, 2006). It is fair, then, to say that searching for the connection between the variability of the solar atmosphere and that of our troposphere has become "third-rail science"—not to be touched at any cost. However, searching for such connections remains highly relevant, since there is a clear societal need to increase skill in predicting the state of the atmosphere on timescales that lie between those of weather and climate: that is, seasonal to decadal (National Academies of Sciences, Engineering, and Medicine, 2016).

Recent studies highlighting the presence, and traceability, of the 22 year magnetic cycle of the Sun have revealed the occurrence a new type of event in the solar lexicon—the "Terminator" (Dikpati et al., 2019; Hurd & Cameron, 1984; McIntosh et al., 2019). Stated simply, a terminator is the event that marks the hand-over from one sunspot cycle to the next. It is an abrupt event occurring at the solar equator resulting from the annihilation/cancelation of the oppositely polarized magnetic activity bands at the heart of the 22 years cycle; that is, there is no more old cycle flux left on the disk. Put another way, a terminator is the end of a Hale magnetic cycle. This annihilation appears to globally modify the conditions for magnetic flux to emerge—principally causing the rapid growth of the magnetic system at midsolar latitudes that will be the host for the sunspots of the next sunspot cycle. Our companion paper (McIntosh et al., 2019, hereafter

M2019) highlights the terminators that took place at the end of solar cycles 22 and 23, illustrating that a significant, step-function-like, change in the Sun's radiative proxies took place at the same time over a matter of only a few days. In their analysis, M2019 demonstrate that terminators were visible in standard proxies of solar activity going back many decades—as many as 140 years to the dawn of synoptic H-α filament and sunspot observations. Dikpati et al. (2019) suggested that the most plausible mechanism for rapid transport of information from the equatorial termination of the old cycle's activity bands (of opposite polarity in opposite hemispheres) to the mid-latitudes to trigger new-cycle growth was a solar "tsunami" in the solar tachocline that migrates poleward with a gravity wave speed (~300 km s^{-1}).

In the following analysis, we will explore *if* these termination events could provide a starting point in establishing a robust Sun-Troposphere connection on decadal timescales, by creating or demonstrating a new fiducial time for solar activity. Correlation does not imply causation, but such a strong correspondence requires explanation, one that is beyond the current paradigm of atmospheric modeling.

2. Observations

The following analysis explores the signature of solar terminators and explores temporal relationships with the episodes of largest fluctuation in the El Niño Southern Oscillation, the so-called El Niño "events." Methodically assessing the solar observations, we will highlight the radiative and particulate signatures of the two best sampled termination events—the two most recent in 1997 and 2010–2011. Using standard measures of solar variability over decades, we can extend to the dawn of the space age—where the proxy data is most reliable. Following the introduction of a data-inspired schematic view of the Sun's 22 years magnetic activity cycle over that same, we will draw comparison with the ocean index. Employing a modified version of the Superposed Epoch Analysis (SEA, Chree, 1913; see Appendix) which takes advantage of this new fiducial time for solar activity, we will not only see how solar, and solar-related, activity "stacks up," we will identify a repeated pattern in the ocean index at those times indicating that there may indeed be a strong connection between the two systems on that timescale.

2.1. Diagnostics of the 1997 and 2011 Terminators

Figure 1 shows a combination of the primary measure used in M2019, the EUV Brightpoint (BP) density as a function of solar latitude. With the variation of the hemispheric variability of sunspots (SILSO World Data Center, 1960–2020, Panel G), and other canonical measures of solar output. The dramatic drop in BP density at the solar equator is visible in 1997 and 2011. Due to the higher quality data coming from the AIA instrument on the Solar Dynamics Observatory (SDO/AIA; Lemen et al., 2012) compared to its predecessor (SOHO/EIT; Delaboudinière et al., 1995), the corresponding midlatitude increases in activity beyond the 2011 termination are more pronounced that in 1997. Progressing down the figure, we see the computed Heliospheric Current Sheet (HCS) tilt angle from the Wilcox Solar Observatory (Panel B; Scherrer et al., 1977; Wilcox et al., 1980) and the Penticton 10.7 cm radio flux (Panel C; Tapping, 2013). The F10.7 flux is considered canonical as it is the longest consistent, calibrated, physical (as opposed to the more subjective counting of sunspots), record of solar activity, stretching back to 1947. Panel D shows the anticorrelated variation of the galactic cosmic-ray flux (CRF) as measured at the University of Oulu's Sodankyla Geophysical Observatory. The anticorrelation of CRF and solar activity (Forbush, 1954; McIntosh et al., 2013) is a result of changes in the Sun's global magnetic field strength (and structural configuration)—basically, a strong solar magnetic field blocks cosmic rays from entering the solar system, and hence the Earth's atmosphere with corresponding increases when said magnetic field is weak. Note that solar cycle 24 has seen a weaker global solar magnetic field than its predecessor, and correspondingly higher cosmic-ray fluxes. Observations of radiative proxies of solar activity from other wavelengths follow, in Panel E, the 1–8 Å integrated coronal X-ray irradiance measured by the GOES family of spacecraft (Chamberlin et al., 2009) and the University of Bremen's composite index of the Sun's chromospheric variability measured through the ultraviolet emission of singly ionized Magnesium (Panel F; Snow et al., 2014). The GOES X-ray flux was the measure in in which terminator events were first detected (Saba et al., 2005; Strong & Saba, 2009). Throughout all panels, the pairs of vertical dotted lines mark step-function changes are present in each of the measured quantities (radiative increases and CRF decreases) that persist for the next several months at the end of Cycle 22 and at the end of Cycle 23.

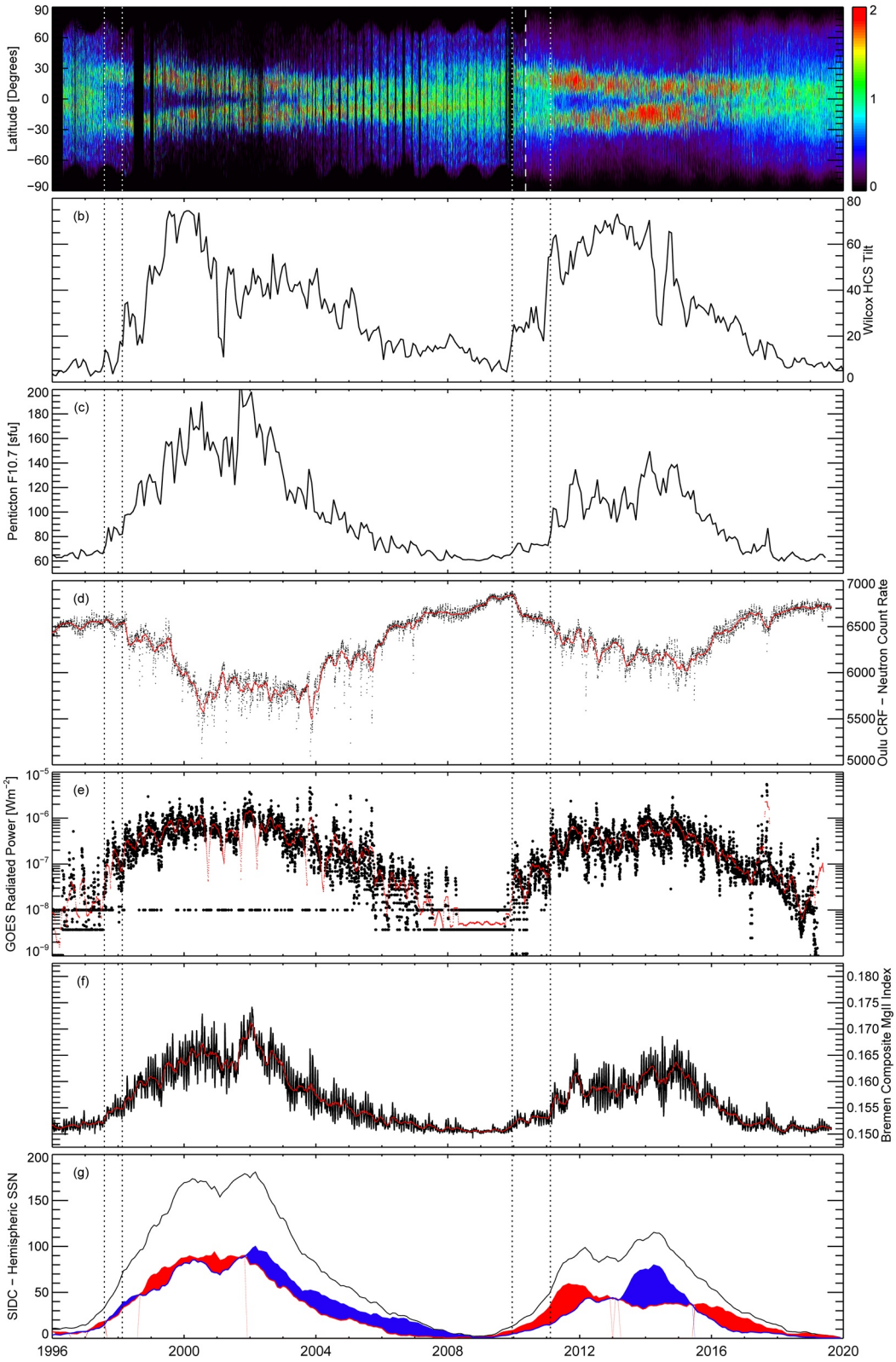
Latitude [Degrees]
(b)
Wilcox HCS Tilt
(c)
Penticton F10.7 [sfu]
(d)
Oulu CRF – Neutron Count Rate
(e)
GOES Radiated Power [Wm^{-2}]
(f)
Bremen Composite MgII Index
(g)
SIDC – Hemispheric SSN
1996
2000
2004
2008
2012
2016
2020

August 1997 and February 2011 are the reported terminator dates from M2019; the other two, March 1998 and December 2009 show coherent correlated step functions in those quantities that do not change at the terminators. For instance, December 2009 shows sharp changes in the tilt of the HCS, GOES X-ray flux, and Oulu cosmic-ray flux, whereas the less energetic photons and sunspots and brightpoints do not rise until the terminator. We surmise that the all the changes are due to two manifestations of the rise of the new solar cycle, perhaps at lower and higher latitudes, for instance, or two injections of magnetic flux from the solar interior driven by magnetized Rossby waves propagating in the solar tachocline (McIntosh et al., 2017) with the first "priming the pump" for the onset of (sunspot) activity. For both solar cycles (in March 1998 and December 2009) the large (∼4%) decrease in cosmic-ray flux is coincident with HCS tilt angle rising over about 20°, which is expected given the discussion about the global structure of the heliospheric magnetic field above (Forbush, 1954). All the panels of Figure 1 suggest that conditions in late 2019 are similar to 2009–2010, suggesting that Cycle 24 is (was) a relatively short cycle, consistent with Leamon et al. (2020).

2.2. Terminators and Spectral Irradiance

When assessing the impact of the Sun's variability on the Earth's atmosphere the primary culprit has been traditionally thought of as the solar cycle related changes in our star's spectral irradiance and its (clear) impact on the regions of the atmosphere above the stratosphere somehow coupling downward (Gray et al., 2010). Through the Sun-as-a-star measurements of the EUV Variability Experiment on Solar Dynamics Observatory (SDO/EVE; Woods et al., 2012) in 2011, we may observe the spectral variability of a termination event like never before. Figure 2 shows the variation in several EVE measures across the first 2 years of the SDO mission, including the 2011 termination. Arranged, from bottom to top, by temperature of formation from (relatively) cool transition region emission in He ii (singly ionized Helium), to the hottest coronal emission of Fe xviii (17 times ionized Iron). The ratio of the pretermination and posttermination emission across that temperature range scales from 8% to 85% and is highly localized with plasma emission around five million Kelvin. This behavior has been noted also by two recent studies (Morgan & Taroyan, 2017; Schonfeld et al., 2017). Figure 2 shows that highly optimized coronal emission starts immediately following February 11, 2011 (the black dashed vertical line). For contrast, in Figure 3, we show the EVE data in a format to illustrate longitudinal behavior on the Sun in the 1215 Å ("Lyman α") and the Fe xvi 335 Å lines—at the peak of the emission increase shown in Figure 2. The time series of EVE data have been arranged in 27 days strips to approximate that of a complete solar rotation—a day of rotation relates to ∼13 degrees of longitude. In the cases shown (that bracket the range of plasma temperatures accessible to EVE) we see that, posttermination, the activity of the Sun exhibits a global "switch-on," that must be related to the global increase in magnetic flux emergence discussed by M2019. To recap, termination exhibits a ∼4% decrease in the CRF and an 8–85% (from low to high temperature emission) increase in the ultraviolet photons that bathe our planet over *only* a few days—significantly less than one solar rotation.

2.3. Terminators in Recent History

Figure 4 continues, and extends, our presentation of solar activity markers and proxies back over the past 60 years. We directly compare the variability of the total and hemispheric sunspot numbers with the latitudinal distribution of sunspots (the so-called "butterfly" diagram). Note that the terminator points, the family of vertical dashed black lines threading the panels of the plot (as developed in M2014) largely align with the very edges of the butterfly wings, noting that we do not use the symbol size in panel B to indicate the size of the spot—only that one was present. Panels c and d are extensions of those presented in Figure 1

Figure 1. Correlated variability of the Sun's output before and after the termination of solar cycles 22 and 23 in 1997 and February of 2011. From top to bottom: (a) the distribution of coronal EUV bright points as a function of latitude and time; (b) the computed tilt angle of the Heliospheric Current Sheet from Wilcox Solar Observatory; (c) the Penticton 10.7 cm radio flux; (d) the cosmic-ray flux as detected at Earth by the Oulu neutron monitor; (e) the integrated 1–8 Å X-ray solar luminosity from the family of GOES spacecraft; (f) the Mg ii index of ultraviolet variability from the University of Bremen; and (g) the hemispheric sunspot number, as recorded by the Royal Observatory of Belgium. The dashed vertical white line in panel (a) represents the transition from SOHO/EIT to SDO/AIA data in May 2010. Notice that during solar minima the X-ray flux in panel (e) can fail to exceed the noise floor of the instrument, and in panel (g) the red and blue traces correspond to the northern and southern numbers, respectively; colored fill corresponds to a dominance of the corresponding hemisphere over the other. SDO/AIA, AIA instrument on the Solar Dynamics Observatory.

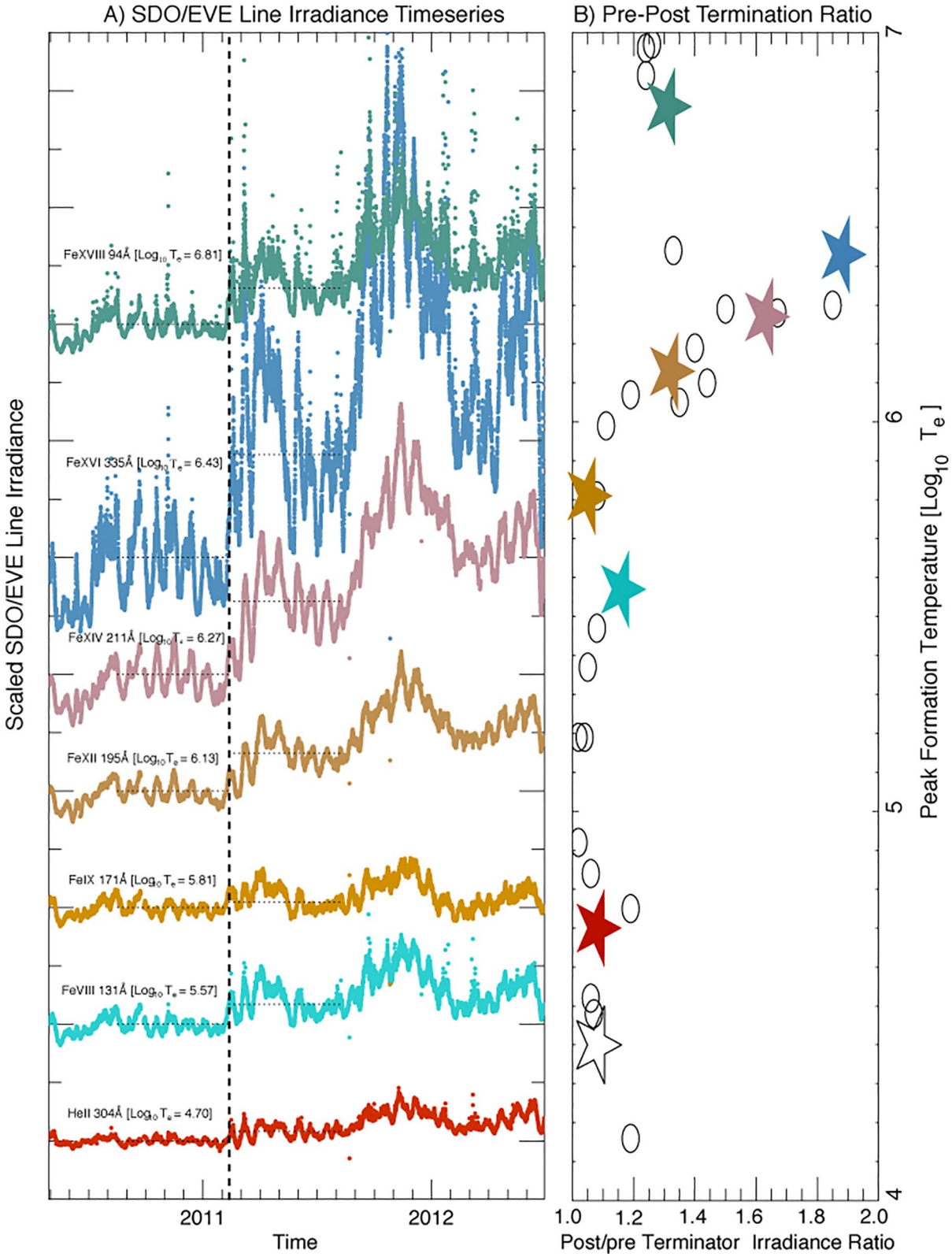
A) SDO/EVE Line Irradiance Timeseries
B) Pre-Post Termination Ratio
Scaled SDO/EVE Line Irradiance
FeXVIII 94Å [Log10 Te = 6.81]
FeXVI 335Å [Log10 Te = 6.43]
FeXIV 211Å [Log10 Te = 6.27]
FeXII 195Å [Log10 Te = 6.13]
FeIX 171Å [Log10 Te = 5.81]
FeVIII 131Å [Log10 Te = 5.57]
HeII 304Å [Log10 Te = 4.70]
2011
2012
Time
1.0
1.2
1.4
1.6
1.8
2.0
Post/pre Terminator Irradiance Ratio
4
5
6
7
Peak Formation Temperature [Log10 Te]

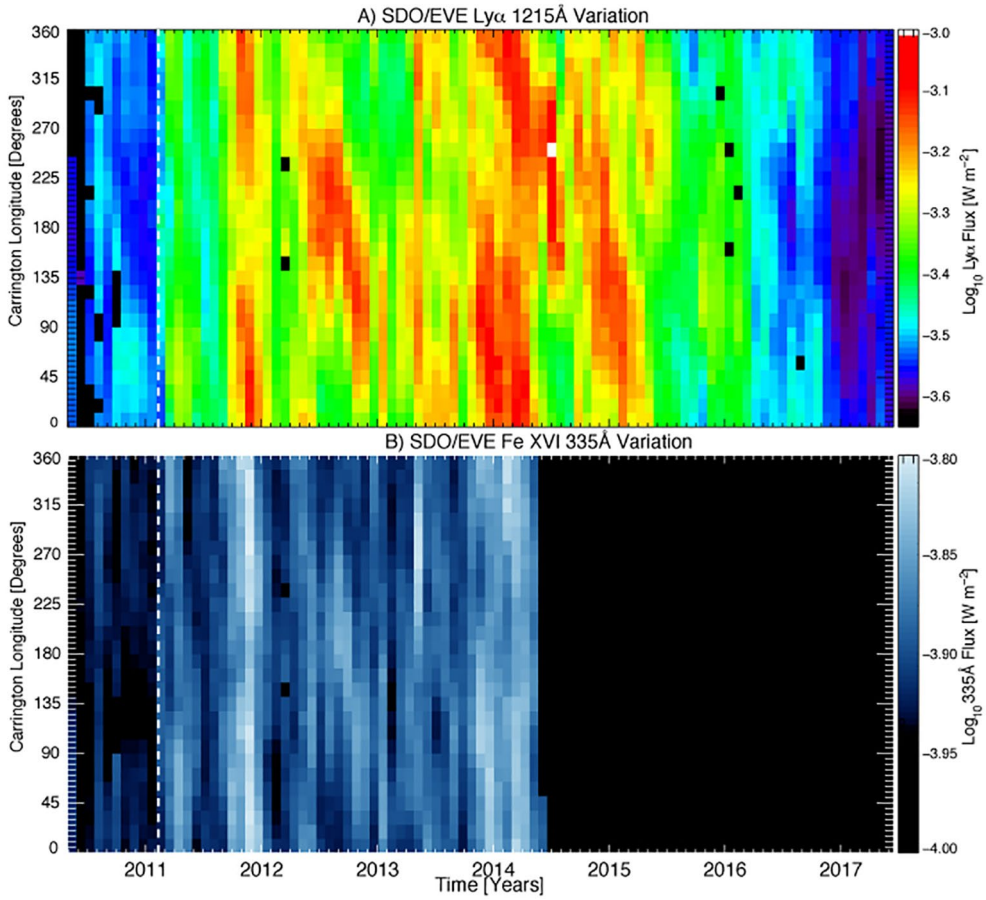

Figure 3. Synthesizing the longitudinal evolution of SDO/EVE measures of the Sun's spectral irradiance. (a) Lyman-α emission from SDO/EVE as a function of Carrington Longitude and time for the whole SDO mission. The onset of emission at the terminator (dashed vertical line) in February 2011 is clear—and global. (b) Similarly, for Fe xvi 335 Å emission, which, per Figure 2a, has the biggest step increase in emission over the terminator of the AIA lines. Note that the short-wavelength detector of EVE was only fully functional until May 2014. SDO/EVE, EUV Variability Experiment on Solar Dynamics Observatory.

where the reader can appreciate the bracketing of the cycles provided by the termination points. Finally, panel e shows a data-motivated depiction of the latitudinal progression of the Sun's magnetic cycle bands.

We introduced the concept of the data-driven SOHO/SDO band-o-gram in our 2014 paper (McIntosh et al., 2014, hereafter M2014), specifically Section 3 and Figure 8 of that paper. There are only three parameters that define each cycle: the time of max of the *preceding* cycle, that is, the time at which new-cycle flux appears at 55° *in each hemisphere*; and the termination point. Since the launch of SOHO, the termination points of cycles 22 and 23 have been observed, and the maxima of cycles 23 and 24, which are origination points of cycles 24 and 25. The bands of flux are assumed to move at a constant angular velocity ($\sim$3° yr^{-1}); this is not strictly accurate, but for such a simple cartoon model it works surprisingly well. One may also extend the model forwards or backwards in times in steps of 22 years; again see Figures 12, 14 and Table 1 of the M2014, and its extensions (McIntosh & Leamon, 2015, 2017). Above 55° latitude, we prescribe a linear progression of 10° per year, in keeping with "Rush to the Poles" seen in coronal green line data

Figure 2. The evolution of constituents of the Sun's spectral irradiance across the 2011 terminator as measured by SDO/EVE. (a) Time series of EVE emission of the seven AIA band passes, scaled to the time interval 180–60 days prior to the terminator. From bottom to top, the lines increase in their formation temperature. Each successively hotter line is offset on the *y*-axis by unity, except for the hottest line—Fe xviii 94 Å—which is offset by two to show the huge increase in emission in Fe xvi 335 Å. (b) The ratio of EVE emission across the terminator as a function of mean formation temperature for the spectral line. The step increase in emission is most pronounced from $\log_{10}T_e = 6.0$–6.4; but even the hottest lines do show a greater increase than lines cooler than 1 MK. SDO/EVE, EUV Variability Experiment on Solar Dynamics Observatory.

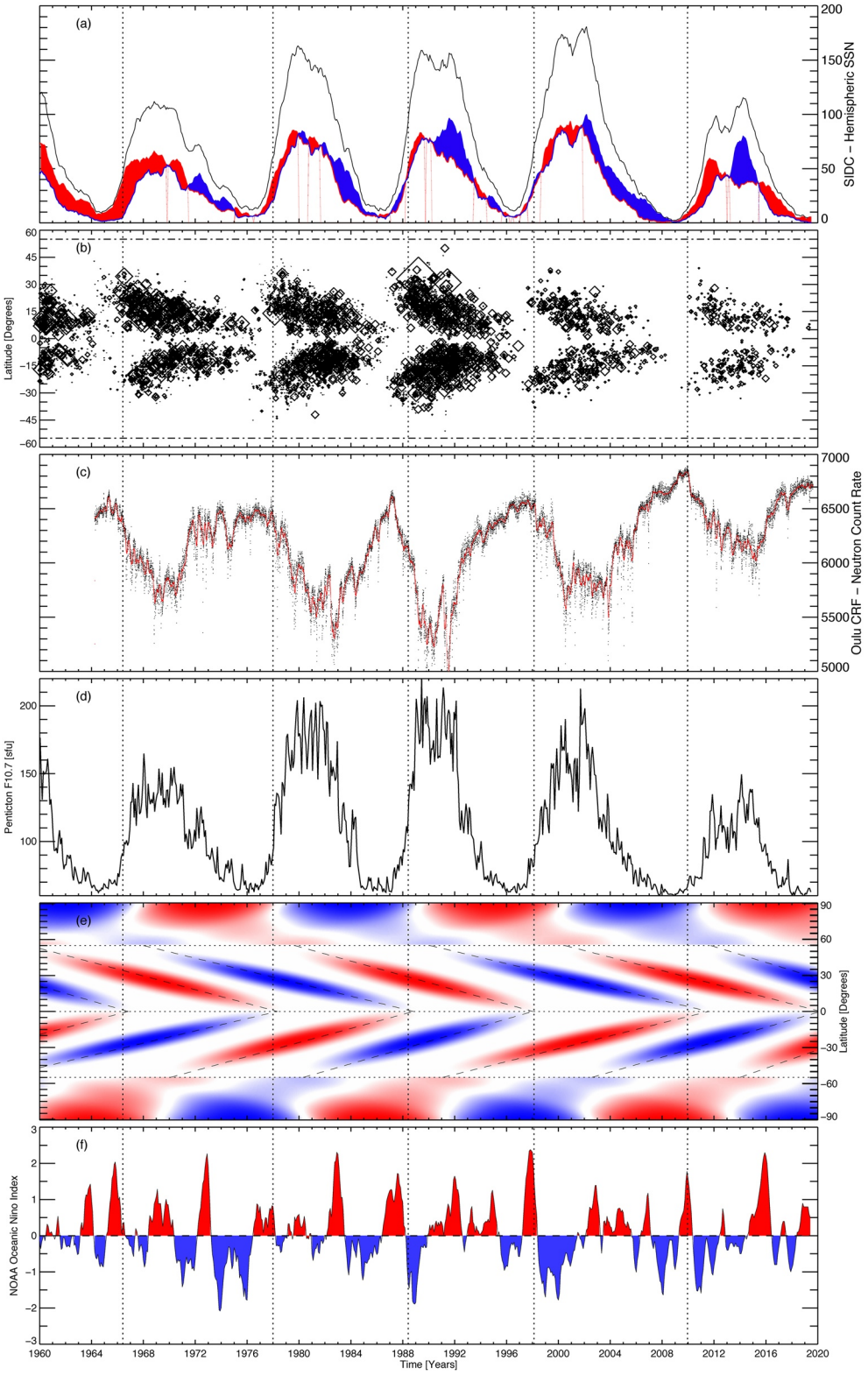

Figure 4. Comparing more than five decades of solar evolution and activity proxies. From top to bottom: (a) the total (black) and hemispheric sunspot numbers (north—red, and blue—south); (b) the latitude-time variation of sunspot locations; (c) the Oulu cosmic-ray flux; (d) the Penticton F10.7 cm radio flux; (e) a data-motivated schematic depiction of the Sun's 22 years magnetic activity cycle; and (f) the variability of the Oceanic Niño Index (ONI) over the same epoch. The black dashed lines mark the cycle terminators.

(Altrock, 1997). M2014 deduced that the temporal overlap and interaction between the oppositely polarized bands of the band-o-gram inside a hemisphere, and across the equator, was the critical factor in moderating sunspot production and establishes the butterfly diagram as a byproduct. The terminator is given as the time that the oppositely polarized equatorial bands cancel or annihilate and establish growth on the remaining midlatitude bands. This gross modification of the Sun's global magnetic field has an impulsive growth on radiative proxies and a corresponding, inverse, relationship on the CRF as shown in Figure 1.

2.4. Terminators and Oceanic Flips

The final two panels of Figure 4 compare the data-motivated band-o-gram with a measure of the El Niño Southern Oscillation (ENSO). There exist various indices to describe ENSO which include or exclude various components; we focus here on the National Oceanic and Atmospheric Administration (NOAA)-generated "Oceanic Niño Index" (ONI). Note that in this paper, we are not trying to explore every bump and wiggle in the ONI—our primary focus are the "decadal-scale" large transitions from El Niño (hot mid-Pacific) to La Niña (cold mid-Pacific), the signature "El Niño Events" like that in 1997–1998 (Trenberth & Stepaniak, 2001). A visual comparison between the termination points in the solar data panels and the ENSO/ONI record would appear to indicate that there is a possible relationship between the termination points and positive-to-negative swings in the ONI record. Just as we not trying to explore every bump and wiggle, we do not try to predict or understand the magnitude of that swing, just that it exists.

To explore this potential relationship a little more we employ a modified Superposed Epoch Analysis (mSEA) to the solar and atmospheric data presented above over the past 60 years. Rather than defining a standard superposed epoch analysis repeating over some number of days/years, the critical modification here is to first scale time to be fractions of a cycle, from terminator to terminator. (One may think of this then as a "phase" of the solar cycle, but we choose here to express length in terms of a fraction 0–1 rather than 0–2π.) The concept of the mSEA is discussed in greater detail in Appendix A2.

The lowest four panels of Figure 5 compare, from bottom to top, the hemispheric sunspot numbers, CRF, Penticton 10.7 cm radio flux, and the NOAA ONI ENSO index. The top two panels replace the band-o-gram of Figure 4 with the NGDC composite Coronal Green Line data (Rybansky et al., 1994) and the Wilcox (HCS) tilt angle from Figure 1. Note that the Wilcox Solar Observatory has only been extant since 1976, so there are only four traces shown for the four cycles 21–24. The clearest feature of the plot is that the mSEA indicates the ONI time series appears to collapse into a coherent regular behavior around the terminators. The consistent pattern of pretermination warming with a rapid transition to a period of cooling following the terminator. Each of these phases last around $x = 0.08$ in the normalized timescale, or about 10–11 months if the interterminator spacing is 11 years or so. This would appear to indicate that in the depths of solar minimum conditions, when the radiative proxies are low and the CRF is high, there are epochs of warm Pacific conditions. Conversely, following the terminator, the rapid growth of radiative proxies and decline of the CRF would appear to systematically correspond to epochs of cooler Pacific conditions. There is a general upward trend (with considerable scatter) in Pacific Ocean temperatures as the solar activity cycle progresses. The scatter appears not inconsistent with the period of a Rossby wave either propagating in the solar tachocline (McIntosh et al., 2017), and clearly visible in the F10.7 flux panel of Figure 5, or across the Pacific Ocean (Meyers, 1979). However, after solar maximum (which in this framework occurs at $x \simeq 0.2$) a pattern returns: three of the five cycles have a coherent second peak (El Niño) at around $x = 0.5$, that is, a couple of years after sunspot maximum; the other two cycles, 22 and 23, have coherent double peaks around $x = 0.33$ and $x = 0.67$—recall that these are the two cycles with the largest offsets between maximum in the northern and southern hemispheres.

While there is small rise in F10.7 flux at the terminator, there is a consistently larger step one tachocline Rossby period later (the $x = 0.08$ vertical dotted line exists to guide the eye). F10.7 also shows a consistent sharp dropoff at $x \sim 0.4$. Sunspot minimum occurs (at $x \simeq 0.8$) when the four activity bands are of equal intensity (McIntosh et al., 2014, cf. Figure 4e here). At the nadir of solar activity, as determined by either SSN or F10.7, we see the start of the coherent preterminator rise to El Niño in the ONI time series, while the CRF, which has been increasing since $x \sim 0.5$, continues to rise until the terminator.

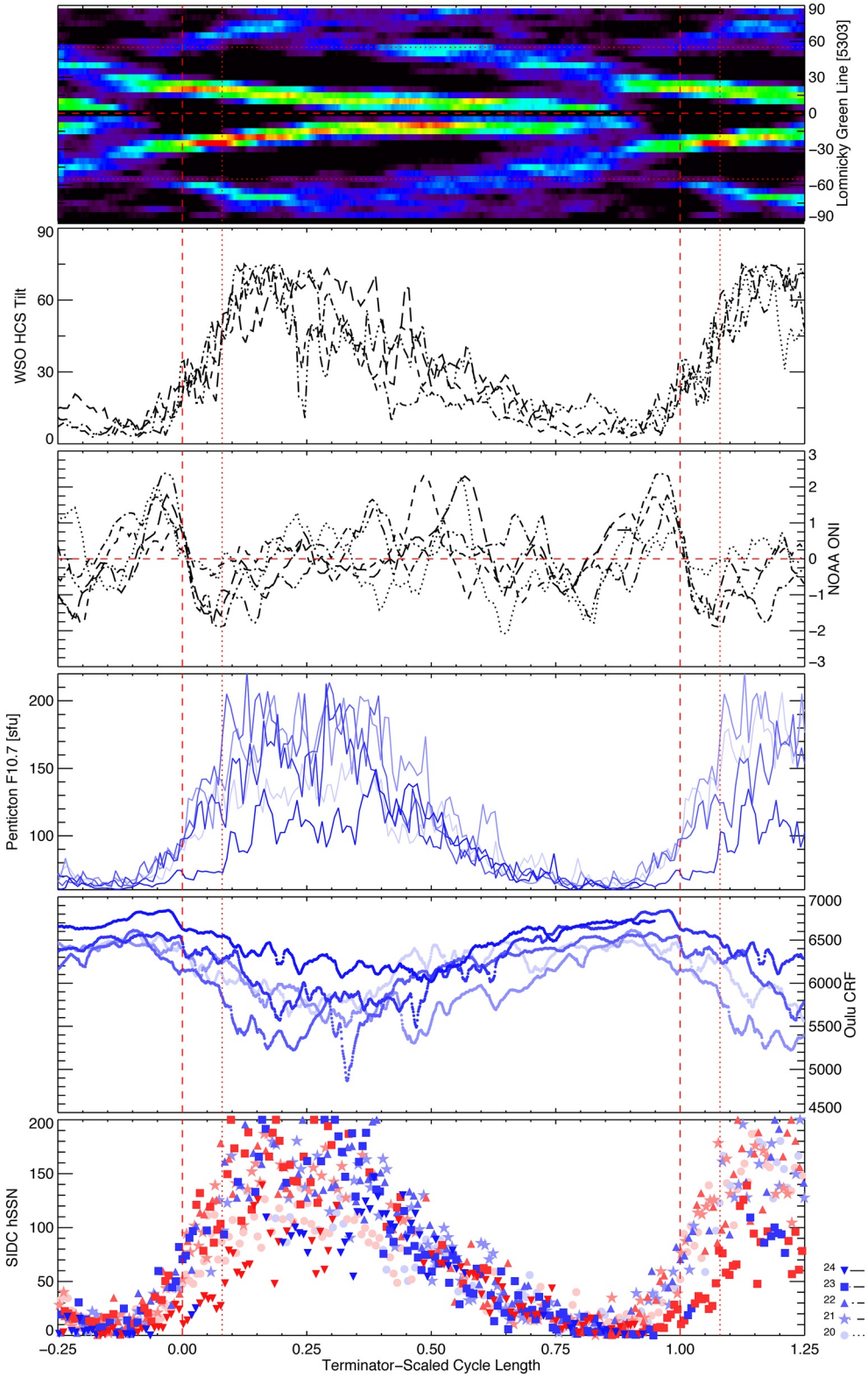
Lomnicky Green Line [5303]
WSO HCS Tilt
NOAA ONI
Penticton F10.7 [sfu]
Oulu CRF
SIDC hSSN
Terminator–Scaled Cycle Length

Taking all the panels of Figure 5 together, the large-scale solar magnetic field, as evidenced by its effect on cosmic-ray propagation and the change in tilt angle of the heliospheric current sheet, appears to better coincide with ENSO shifts near the terminators than changes in solar photons.

3. Discussion

In the previous section, we have made use of a modified Superposed Epoch Analysis (mSEA) to investigate the relationships between solar activity measures and variability in a standard measure of the variability in the Earth's largest ocean—the Pacific. We have observed that this mSEA method brackets solar activity and correspondingly systematic transitions from warm-to-cool Pacific conditions around abrupt changes in solar activity we have labeled termination points. These termination points mark the transition from one solar activity (sunspot) cycle to the next following the cancellation or annihilation of the previous cycle's magnetic flux at the solar equator—the end of Hale magnetic cycles.

Correlation does not imply causation; however, the recurrent nature of the ONI signal in the terminator fiducial would appear to indicate a strong physical connection between the two systems. Appendix B discusses three statistical Monte Carlo tests that show the chances of these events lining up for five cycles are remote: in summary we may reject the null hypothesis of random cooccurrences with a confidence level $p < 3.4 \times 10^{-3}$. We do not present an exhaustive set of solar activity proxies, but it would appear that the CRF, as the measure displaying the highest variability, as something to be explored in greater detail in coupled climate system models.

There have been many possible explanations postulated for a cosmic-ray climate connection, including: (i) Forbush decreases inducing increased extratropical storm vorticity (Roberts & Olson, 1973; Tinsley et al., 1989) and atmospheric gravity waves propagating from the auroral ionosphere (Prikryl et al., 2009); (ii) global electric conductivity inducing changes in cloud microphysics (Harrison, 2004; Tinsley, 2000); and (iii) direct formation of ionization particles seeding cloud formation (Svensmark & Friis-Christensen, 1997; Svensmark et al., 2017). However, the effects of cosmic rays on cloud formation are a matter of hot debate (e.g., Gray et al., 2010; Kristjánsson et al., 2002; Pierce, 2017), with even the sign of the correlation between cosmic rays and climate not agreed on. For all the debate these explanations have generated, they are all *irrelevant* in terms of the correlations and empirical predictions we discuss here.

Independent of the exact mechanisms of coupling solar modulation to ENSO, which are beyond the scope of this manuscript, the results discussed above and shown in Figure 5 hold for the past five solar cycles, or 60 or so years. The question must be asked, then, why has the regular pattern of Figure 5 occurred and reoccurred regularly since 1966?

As Figure 4 shows, we only have continuous cosmic-ray observations from 1964, just before the cycle 19 terminator. The F10.7 record extends back to 1947 (near the peak of cycle 17), but Pacific Sea Surface temperatures and sunspot areas extend to the 1870s. Other than the 1915 termination of solar cycle 14, there is little evidence for such a correlation prior to the events discussed here. (Cycle 14 was notably the weakest cycle of the twentieth Century, and thus almost certainly had the highest CRF prior to the continuous observation record.) However, there certainly have been changes in the Earth's atmosphere over the twentieth Century...

Figure 5. A modified superposed epoch analysis (mSEA) applied to the data shown in Figures 1 and 4 for the last five cycles (note symbol key to lower right). The terminator is marked by the red dashed line at $x = 0$ (and repeated at $x = 1$), and its signature is clearly simultaneously visible in solar, heliospheric *AND* atmospheric data. The bottom panel shows the SIDC monthly sunspot number, color-coded red or blue depending on which hemisphere is dominant. The second panel shows the Oulu Cosmic-Ray Flux. Note the coordinated 3%–5% decrease around $x = 0$. The third panel shows the Penticton F10.7 flux. The turn-on (and subsequent turn-off) with the phase of the cycle is remarkably consistent over the cycles 20–24, at around $x = 0.08$ and $x = 0.4$; $x \sim 0.08$ is consistent with the period of a Rossby wave propagating in the solar tachocline (McIntosh et al., 2017). The fourth panel shows the NOAA ONI ENSO index: the change from El Niño to La Niña at the terminator is striking. The coherent behavior of all quantities (that is, more coherent than SSN) with the phase of the cycle is clear over cycles 20–24. NOAA ONI ENSO, National Oceanic and Atmospheric Administration Oceanic Niño Index El Nino Southern Oscillation.

3.1. Atmospheric Changes

It is probably not a coincidence that the period of terminator-ENSO correlation corresponds to the close-to-monotonic rise in global sea surface temperatures over the same time period as Figure 4 (the "hockey stick" graph). Tropospheric warming leads to stratospheric cooling (Ramaswamy et al., 2006); do the effects of a colder stratosphere on the physical and chemical processes in it make it more susceptible to amplifying transient changes in solar input? Further, since about 1945, the Pacific Decadal Oscillation (Mantua et al., 1997) has been in a predominantly negative phase, the feedback to net irradiance from clouds has been increasingly negative (Zhou et al., 2016), and a ~4%–6% decrease in cloud cover over the western Pacific (~140–160°E) has been reported from ship-borne observations since 1954, with a comparable increase over the mid-Pacific (~150–120°W; Bellomo et al., 2014). Note that 160°E is the "balance point" about which warm and cold SSTs flip in an El Niño-La Niña transition (Pinker et al., 2017).

Thus, over the past several decades the cloud pattern in the western Pacific has adopted an almost El Niño-like default state, consistent with an observed eastward shift in precipitation in the tropical Pacific and weakening of the Walker circulation over the last century (Deser et al., 2004; Vecchi & Soden, 2007a), and which has been tied, via simple thermodynamics, to a warmer atmosphere. Over the same past four decades timeframe, evidence for a changing Brewer-Dobson circulation—the mass exchange between troposphere and stratosphere characterized by persistent upwelling of air in the tropics—comes from satellite and radiosonde data, which indicate a reduction in temperatures and ozone and water vapor concentrations, particularly in the tropical lower stratosphere at all longitudes (Thompson & Solomon, 2005), pointing to an accelerated tropical upwelling (Rosenlof & Reid, 2008). Domeisen et al. (2019) discuss the teleconnection of ENSO both vertically, to the stratosphere, and thence latitudinally affecting the strength and variability of the stratospheric polar vortex in the high latitudes of both hemispheres: El Niño events are associated warming and weakening of the polar vortex in the polar stratosphere of both hemispheres, while a cooling can be observed in the tropical lower stratosphere. These impacts are linked by a strengthened Brewer-Dobson circulation, with planetary waves generated by latent heat release from tropical thunderstorms being the likely modulation mechanism (Deckert & Dameris, 2008; Domeisen et al., 2019).

Thus, it is entirely plausible that since changes in the (upper) atmosphere brought on by a strengthened Brewer-Dobson circulation, weakened Pacific Walker circulation, and less cloudy Western Pacific, enables the relatively constant terminator-driven changes to have sufficient "impact" to flip the system from El Niño to La Niña, independent of the actual mechanism that couples solar changes to clouds and ENSO. Such circulation changes are only likely to intensify in a future with higher tropical heat and moisture at the sea surface, affecting not only tropospheric climate but also stratospheric dynamics.

3.2. Socioeconomic Implications

Forecasting ENSO and its related climate variations is a high-stakes societal imperative given that El Niño impacts "lives, property, and economic activity around the globe" (McPhaden, 2015). For instance, as an example of not necessarily being concerned about why or how an empirical relationship works from a forecast standpoint, Smith et al. (2016) noted "An ability to forecast the time-averaged NAO months to years ahead would be of great societal benefit, but current operational seasonal forecasts show little skill." Dunstone et al. (2016) thus improved the skill of 12 months ahead NAO forecasts when an 11 years (solar cycle) parameterized solar irradiance forcing term was added. Smith et al. and Dunstone et al. focused on the severity of the British winter, primarily from the viewpoint of the energy and insurance sectors.

Directly focused on catastrophic ENSO impacts, flooding in Australia during the 2010–2012 La Niñas and the ensuing economic cleanup costs (A$5–10 billion (US$4.9–9.8 billion) in Queensland alone) led to the commissioning of a Government Report on "two of the most significant events in Australia's recorded meteorological history" (Bureau of Meteorology, 2012). Similarly, the Peruvian government estimated the very strong 1997–1998 El Niño event cost about US$3.5 billion, or about 5% of their gross domestic product (GDP). Globally, United Nations estimates of El Niño-related damage from the same event ranged from US$32 to US$96 billion. In the United States, NOAA assessed direct economic losses from that event likely exceeded US$10 billion (Weiher, 1999).

The mild winters and greater than average rainfall to the Southwest in El Niño years save US energy consumers US$2.2 billion less in fuel heating costs (Teisberg, 1999); however, the savings is lost in La Niña years with more sever winters. Agriculture is the most climate sensitive industry and climate is the primary determinant of agricultural productivity. Estimates of the impacts on U.S. agriculture of the 1997–1998 El Niño and the 1998–1999 La Niña; those losses range from US$1.5–$1.7 billion from El Niño and US$2.2–$6.5 billion from La Niña (Chen et al., 2001; Weiher & Kite-Powell, 1999). That assessment comes with the important caveat that losses associated with El Niño-related floods or droughts in some areas can be offset by gains elsewhere, for instance through reduced North Atlantic hurricane activity, lower winter heating bills or better harvests for certain crops—Argentinian wheat yields are strongly increased in El Niño years, for example, whereas US (and moreso Canadian) yields fall (Gutierrez, 2017). Nevertheless, combining the costs of natural disaster recovery with the costs associated with yields of major commodity crops (Gutierrez, 2017; Iizumi et al., 2014), the need to be able to predict ENSO events beyond a seasonal forecast (e.g., https://community.wmo.int/activity-areas/climate/wmo-el-ninola-nina-updates (World Meteorological Organization) is high.

That crop yields in North and South America, Australia, and Eurasia vary, along with regional temperature and precipitation changes, makes it clear that ENSO influences, through "teleconnections," (e.g., Bjerknes, 1969; Domeisen et al., 2019) the global dynamics of seasonal winds, rainfall, and temperature. These teleconnections imply, indeed require, coupling throughout the atmosphere, and despite the mention of troposphere in the title of this paper, manifestations of ENSO are observed throughout the neutral atmosphere and higher.

One final economic impact consideration, also tied to global teleconnections, is the strength of Atlantic hurricane season, which is relatively strong in the first year of La Niña after an El Niño, when waters are still warm but upper-level wind shears are favorable for cyclone genesis (Vecchi & Soden, 2007b). As such, we may expect a particularly active season in 2021, and maybe even 2020, depending on exactly when the terminator and ENSO transition occurs.

4. Conclusion

As discussed in M2014, the band-o-gram developed therein could be extrapolated linearly out in time. The linear extrapolation of the solar activity bands outward in time was verified in McIntosh et al. (2017) by updating the original observational analysis and comparing to the earlier band-o-gram. M2014 projected that sunspot cycle 25 spots would start to appear in 2019 and swell in number following the terminator in mid-2020. Six years later, we are seeing these predictions come true with the first numbered active regions and low level (C-class) flaring activity. Based on the mSEA of the past 60 years, an enduring warm pool in the central and western Pacific at solar minimum (ONI has been consistently positive since early 2018, even though it never got so warm to become a fully fledged strong El Niño event) was not unexpected, and we expect a rapid transition into La Niña conditions later in 2020 following the sunspot cycle 24 terminator. Given the warm waters, we project a particularly active Atlantic hurricane season in 2021, and maybe even 2020, depending on exactly when the terminator and ENSO transition occurs this year.

In conclusion, we have presented clear evidence in Figure 5 of a recurring empirical relationship between ENSO and the end of solar cycles. We have tried to avoid discussion of causation, which, due to its controversial nature could lead to dismissal of the empirical relationship, and we want open a broader scientific discussion of solar coupling to the Earth and its environment. Nevertheless, independent of the exact coupling mechanisms, the question must be asked, why has the pattern occurred and reoccurred regularly for the past five solar cycles, or 60 years? We have only a few months at most to wait to see if this Terminator-ENSO relation continues at the onset of the coming solar cycle 25. Should this next terminator be associated with a swing to La Niña then we must seriously consider the capability of coupled global terrestrial modeling efforts to capture "step-function" events, and assess how complex the Sun-Earth connection is, with particular attention to the relationship between incoming cosmic rays and clouds and precipitation over our oceans. ENSO is the largest mode of atmospheric variability driving extreme weather events with large costs and so *any* improvement in prediction of that would be of societal benefit.

Appendix A: Methods

A1. The Coronal Green Line and Extended Solar Cycle

Starting with the advent of the coronagraph in the late 1930s, routine measurements were made of the 5303 Å "green line" of the corona, even before it was known that it was emission from highly ionized iron (Fe xiv). Multiple researchers, including Wilson et al. (1988), and Altrock (1997); Altrock (2003), showed that the intensity at high latitudes (>60°, or at the very least, higher than the highest observed sunspots) manifested an "extended" solar cycle. Further, the high-latitude emission was situated above the high-latitude neutral line of the large-scale photospheric magnetic field, thus implying a connection with the solar dynamo. All in all, the 5303 Å Green Line observations are an extended duration record providing evidence for an "extended" solar cycle that begins every 11 years but lasts for ~19–20 years. The band-o-gram of Figure 4 implicitly assumes this Wilson-like 19–20 years progression from 55° to equatorial termination.

A2. Modified Superposed Epoch Analysis

The concept of a Superposed Epoch Analysis (SEA) is over a hundred years old (Chree, 1913). It was originally conceived (appropriately enough) for the purpose of correlating sunspots with terrestrial magnetism—the recurrence in geomagnetic data of the 27 days Carrington periodicity. Similar techniques were used by Roberts and Olson (1973) to show the correlation between geomagnetic storms and increased storm vorticity over the Northern Pacific Ocean. Tinsley et al. (1989) extended the earlier storm vorticity analysis, again looking at superposed epochs, but for Forbush decreases (i.e., the Cosmic-Ray Flux decrease associated with a CME, rather than the associated geomagnetic storms. Roberts also discussed the possible amplifying effects of cloud microphysical processes. Recall from Section 2.1 that a 3%–5% drop in GCR flux that occurs at a terminator, which that does not recover; it is not inconceivable that such a change is responsible for changes in large-scale weather patterns in the Pacific Ocean. The terminator dates in Figure 5 are defined from the band-o-gram (solar data), but, motivated by Roberts and Tinsley, are then adjusted by up to ±100 days such that the GCR traces line up (bottom of the drop. Table A1 shows a list of temporal shifts applied.

Recall that the top two panels of the mSEA Figure 5 replaced the band-o-gram of Figure 4 with the computed HCS tilt angle from the Wilcox Solar Observatory for the not quite four cycles that data has been extant (1976-present), and the NGDC composite Coronal Green Line data. To be clear, the data in this panel does not overlap temporally with the other panels of Figure 5 (1939–1989 compared to 1965-present). Nevertheless, as a composite "standard cycle," it provides insight into the changes in, for example, F10.7 emission and GCR flux. For clarity, we track the local maxima in emission, allowing four per hemisphere, and plot the "average track" of peak emissions, as a function of time, and then compile them in an mSEA analysis. Expressing cycle progression as a fraction of their length requires the terminator of cycle 24 to be hard-wired. It is set to be September 1, 2020, based on our current extrapolation of the equatorial progression of EUV BPs (Leamon et al., 2020; McIntosh & Leamon, 2017). If Cycle 24 does not terminate until later, then the corresponding traces in Figure 5 would be compressed leftwards; however, an inspection of the rising

Table A1
Temporal Shifts Applied to EUV BP Terminator Dates to Align to Step Changes in GCR Record

Cycle	Terminator date (Observed)	mSEA temporal Shift (Days)
19	June 1, 1966	0
20	January 1, 1978	0
21	June 1, 1988	−100
22	August 1, 1997	+30
23	December 15, 2009	+100
24	July 1, 2020	—

Note. See Figures 4 and 5.

and falling edges of the F10.7 trace does suggest that late-2020 is an accurate assumption at the time of writing. (This date implies that Cycle 24 is relatively short, at less than 10 years, compared to almost 13.0 years for Cycle 23.) Finally, for completeness, we have remade the Green Line composite mSEA using SSN max and min as the fiducial time; the spread of peak intensity tracks is optimum using the terminators, as shown in Figure 5.

We repeat from the main body Section 3: taken together, the panels of Figure 5 imply that corpuscular radiation—specifically galactic cosmic rays modulated by the large-scale heliospheric magnetic field—appears to have greater influence on ENSO than photons, independent of the exact mechanism by which they couple to the atmosphere.

Appendix B: Terminators and ENSO: Monte Carlo Simulations and Statistical Tests

We can quantify the apparent correlation between terminators and ENSO phase changes by employing three different Monte Carlo simulations.

First, we observe from Figure 4 that there are 13 major El Niño to La Niña transitions (defined as a change of the NOAA ONI index of −1 in less than 12 months) over the duration of the data set; the mean gap between them is 57.4 ± 25.5 months. Repeatedly creating an artificial "ONI" time series akin to Figure 4 with 13 El Niño to La Niña transitions, normally distributed, and computing the mean separation with the closest terminators, we find that in only 40 of 10^6 runs is the mean terminator separation 3 months or less, and in only 1,361 of 10^6 runs is the mean terminator separation 5.6 months or less, where 5.6 months is the mean La Niña lag, uncorrected for Rossby-driven short-term fluctuations (see Table A1). By comparison, over all 10^6 runs the mean terminator separation is 15.7 ± 3.5 months, and the 95% confidence interval (shaded) is [9, 22] months as shown in the left-hand panels of Figure B1. Choosing a Poisson or uniform distribution instead of a normal distribution does not change the overall result, and in fact only decreases the number of runs where the mean terminator separation is less than observed reality—the Poisson distribution, probably the most realistic case, has only two out of 10^6 runs better than reality. This translates to rejection of the random coincidence (null) hypothesis at a p value of 2.5×10^{-4}.

The second Monte Carlo trial divides the observed ONI time series since 1960 into 32 pieces, with each positive-negative zero crossing of the time series defining those pieces. For each trial these pieces are randomly reordered, and the (summed) change in the ONI index from the observed Terminator dates ± 3 months is compared to the observed ONI data. Defining the difference, δONI, as before minus after, such that an El Niño-La Niña swing is positive, $\sum\delta\text{ONI} = +10.26$. Two example Monte Carlo shuffled time series are shown in Figure B2, and the results of all 10^6 runs are shown in the middle column of Figure B1: In only 203 of 10^6 runs is the simulated data better than the historical data, rejecting random coincidence with a confidence $p = 1.0 \times 10^{-4}$. Without the GCR correction (see Table A1), however, the confidence level drops precipitously: the dotted lines in the middle column of Figure B1 are only 0.98 standard deviations above the mean, within the 95% core, and the confidence value is only $p = 0.163$, insufficient for rejection of randomness.

The third Monte Carlo trial again takes the random reordering of 32 pieces of the ONI record, but instead of computing the summed change in the ONI index, which can be skewed by correctly guessing the largest ENSO flips (e.g., 1997–1998), we employ a Hilbert transform phase technique. In signal processing, the Hilbert transform is a specific linear operator that takes a function, $u(t)$ of a real variable and produces another function of a real variable $\mathcal{H}[u(t)]$. This linear operator is given by convolution with the function $1/(\pi t)$. The Hilbert transform has a particularly simple representation in the frequency domain: it imparts a phase shift of 90° to every Fourier component of a function; as such, an alternative interpretation is that the Hilbert transform is a "differential" operator, proportional to the time derivative of $u(t)$. Thus a time series $z(t)$ can be expressed as $z(t) = u(t) + i\mathcal{H}[u(t)] = A(t)\exp[i\phi(t)]$, where $A(t)$ and $\phi(t)$ are the *instantaneous* amplitude and phase functions, respectively, of the time series (Bracewell, 2000; Chapman, Lang, Dendy, Giannone et al., 2018; Pikovsky et al., 2002).

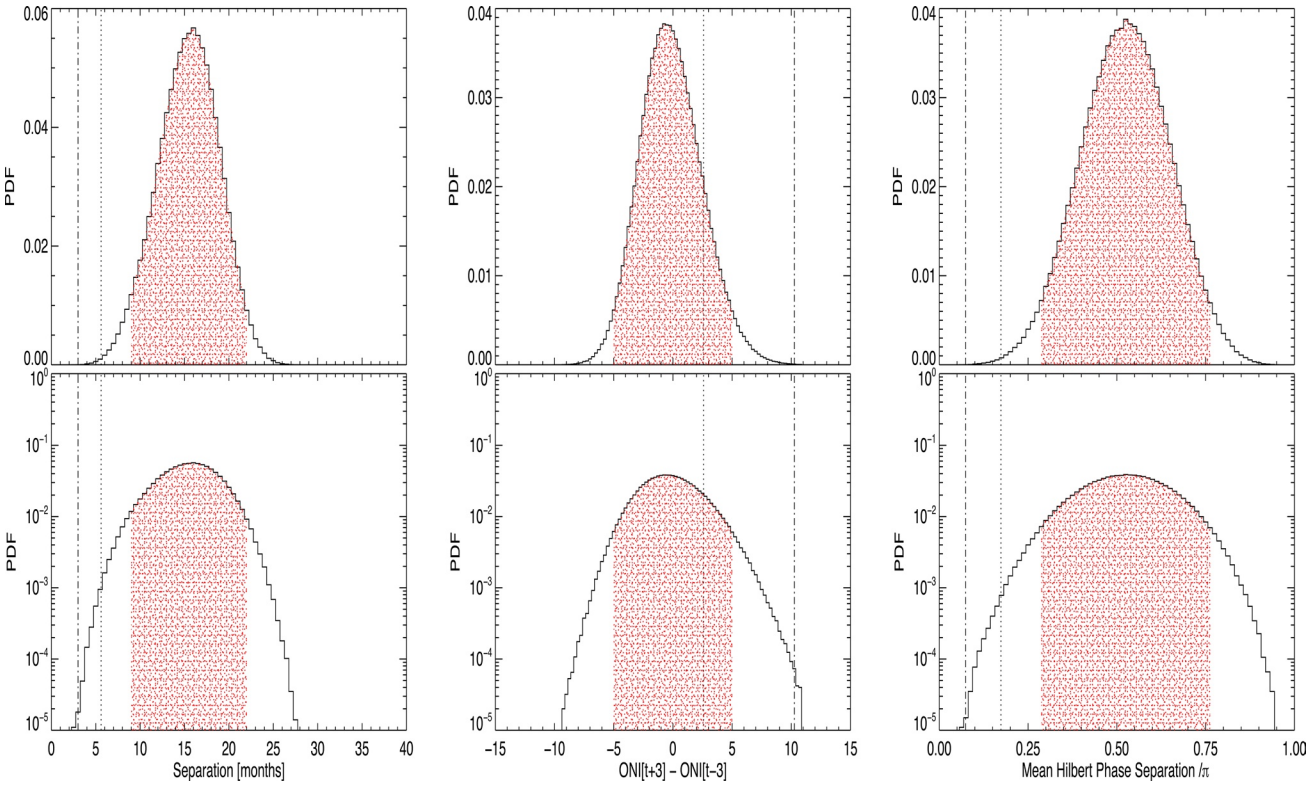

Figure B1. (Left) Monte Carlo test 1: normally distributed (in time) ENSO flips. The dotted line indicates 5.6 months and the dot-dashed line indicates 3.0 months—the observed and GCR-corrected mean terminator-ENSO flip separation (see text); smaller numbers are better. (Middle) Monte Carlo test 2: piecewise-shuffled δONI across terminators. The dotted and dot-dashed lines again indicate the observed and GCR-corrected averages; in this case larger numbers are better. (Right) Monte Carlo test 3: piecewise-shuffled Hilbert phase difference $\delta\phi$ at terminators; smaller numbers are better. In each case there were 10^6 runs, the top panels show the simulation results with a linear y-axis; the bottom panels show the same data on a logarithmic scale, and the red shadings indicate the peak 95% of the distribution (confidence interval). ENSO, El Nino Southern Oscillation; ONI, Oceanic Niño Index.

It is that analytic temporal phase $\phi(t)$ that we refer to above as the Hilbert phase of ENSO variability. A useful feature of the Hilbert phase is in the phase coherence of two time series: if edges/events in one time series occur at constant phase in another, the two are one-to-one correlated, or "phase locked" or "synchronized" (Chapman, Lang, Dendy, Giannone et al., 2018; Chapman, Lang, Dendy, Watkins et al., 2018). Leamon et al. (2020) showed that this Hilbert method could accurately and robustly determine the terminators from sunspot numbers alone.

This technique is used to calculate the mean phase difference between the (shuffled) ONI crossings and the prescribed N terminators, that is, $[\delta\phi(t_0) + \delta\phi(t_1) + \cdots + \delta\phi(t_{n-1})]/N$, where t_n is the time of the nth terminator. The results of this method, for 10^6 Monte Carlo runs are shown in the right-hand panels of Figure B1. The dashed line, the mean phase difference of the five terminators (cycles 19–23), is $(0.074 \pm 0.099)\pi$, and the dotted line describes the upper limit of uncertainty. Only 12 of 10^6 runs in the simulated data are better than the historical 0.074π (and only 1,598 of 10^6 are better than the dotted line, the upper limit of uncertainty at $(0.074 + 0.099)\pi = 0.173\pi$), still far outside the 95% core of the distribution bounded by $[0.29\pi, 0.76\pi]$); we thus reject random coincidence via the Hilbert phase test with a confidence $p = 2.5 \times 10^{-4}$.

In summary, then, combining the results of these three different tests, we can say with a confidence level no less than $p = 3.4 \times 10^{-3}$, the correlation between terminators and ENSO phase changes is *not* a coincidence. That the GCR-corrected timings are better than their original sunspot number record counterparts (especially on test 2) only reinforces the legitimacy of the GCR correlations as discussed in the main body in Sections 3 and 3.1, even though at this point we again acknowledge that correlation is not causality. We reserve the search for potential pathways for future works, particularly if (as) the 2020 La Niña exists.

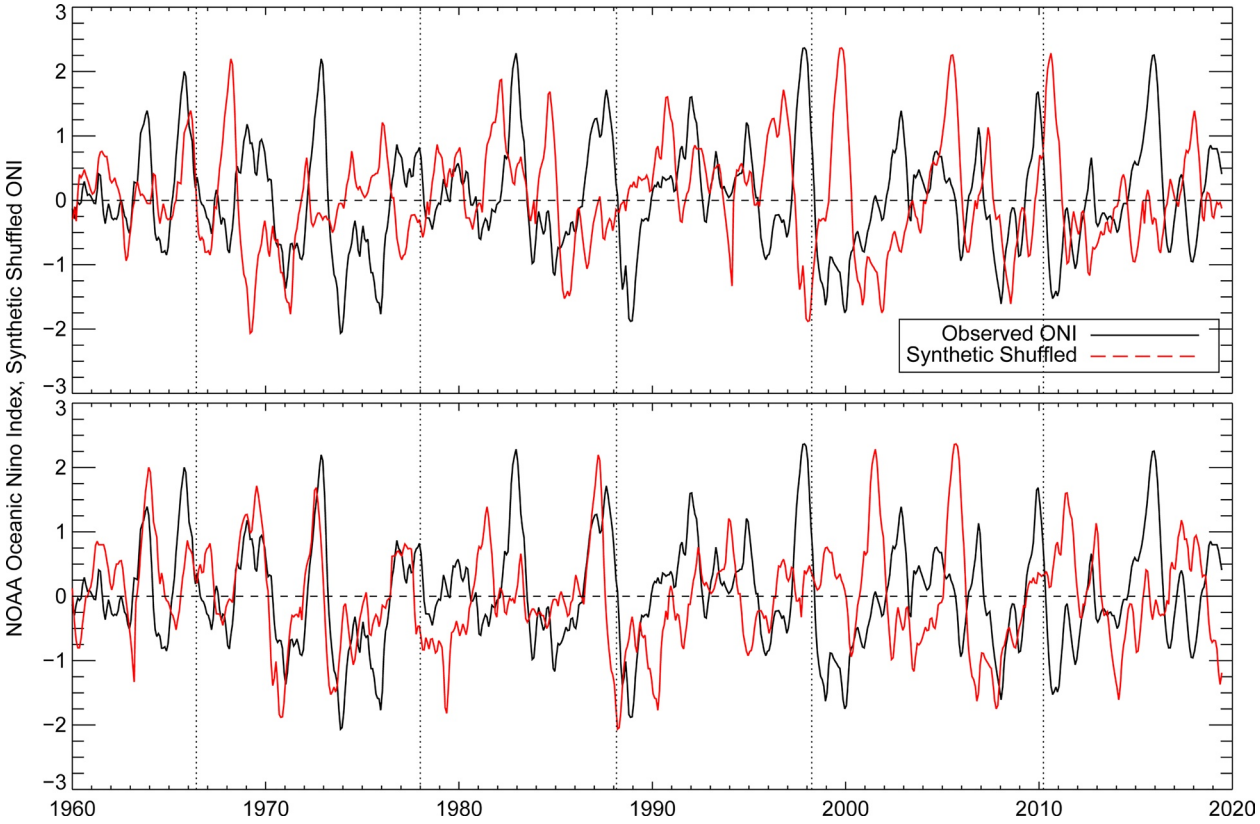

Figure B2. The observed ONI time series from 1950, plus two examples piecewise-shuffled synthetic time series, as used in Monte Carlo tests 2 and 3. The observed terminators are indicated by vertical dashed lines. (top) This particular exemplar lines up well for the 1966 event, but the others are not in phase, and almost exactly out of phase in 1978 and 1988. The summed δONI across the terminators (MC test 2) is −1.09 and the average absolute phase difference (test 3) is $(0.67 \pm 0.36)\pi$. (bottom) One of the only 12 synthetic time series (Figure B1, above) with a better average absolute phase difference (test 3) than the real observed ONI record. The summed δONI across the *observed* terminators (MC test 2) is + 9.54 and the average absolute phase difference (test 3) is 0.069π. Recall the observed historical quantities are + 10.26 and 0.074π for tests 2 and 3, respectively. ONI, Oceanic Niño Index.

Data Availability Statement

All the data presented here are publicly available from their respective archives or observatories, as indicated by the following organizations, institutions, and URLs: From WDC-SILSO, Royal Observatory of Belgium, Brussels, the sunspot number (http://www.sidc.be/silso/datafiles). From NOAA, the Oceanic Niño Index (https://origin.cpc.ncep.noaa.gov/products/analysis/monitoring/ensostuff/ONI/v5.php), the GOES X-ray irradiance (http://www.ngdc.noaa.gov/stp/satellite/goes/index.html), and the Coronal 5303 Å (Fe xiv) "green line" (https://www.ngdc.noaa.gov/stp/solar/corona.html). From the University of Oulu, the Sodankyla Geophysical Observatory record of the cosmic-ray flux (http://cosmicrays.oulu.fi/readme.html). From the Dominion Radio Astrophysical Observatory, Penticton, the F10.7 radio flux (https://spaceweather.gc.ca/solarflux/sx-4-en.php). The EVE (EUV Variability Experiment) spectral irradiance data from the Solar Dynamics Observatory are stored at the University of Colorado (http://lasp.colorado.edu/home/eve/data/data-access/). From the University of Bremen, the Mg ii chromospheric variability index (http://www.iup.uni-bremen.de/UVSAT/Datasets/mgii). From Stanford University, the Wilcox Solar Observatory's Heliospheric current sheet extrpolations (http://wso.stanford.edu/HCS.html).

Acknowledgments
Robert J. Leamon was supported by an award from the NASA Living with a Star program to NASA GSFC. The National Center for Atmospheric Research is sponsored by the National Science Foundation and the compilation of feature databases used was supported by NASA Grant NNX08AU30G. We thank Lesley Gray, Justin Kasper, Kevin Trenberth, Nicholeen Viall, and Sandra Chapman for constructive discussions improving earlier versions of the manuscript.

References

Altrock, R. C. (1997). An 'Extended Solar Cycle' as observed in Fe xiv. *Solar Physics*, *170*, 411–423. https://doi.org/10.1023/A:1004958900477
Altrock, R. C. (2003). Use of ground-based coronal data to predict the date of solar-cycle maximum. *Solar Physics*, *216*, 343–352. https://doi.org/10.1023/A:1026125332040
Bal, S., Schimanke, S., Spangehl, T., & Cubasch, U. (2011). On the robustness of the solar cycle signal in the Pacific region. *Geophysical Research Letters*, *38*, L14809. https://doi.org/10.1029/2011GL047964

Bellomo, K., Clement, A. C., Norris, J. R., & Soden, B. J. (2014). Observational and model estimates of cloud amount feedback over the Indian and Pacific Oceans. *Journal of Climate*, *27*, 925–940. https://doi.org/10.1175/JCLI-D-13-00165.1

Bjerknes, J. (1969). Atmospheric teleconnections from the Equatorial Pacific. *Monthly Weather Review*, *97*(3), 163. https://doi.org/10.1175/1520-0493(1969)097⟨0163:ATFTEP⟩2.3.CO;2

Bracewell, R. N. (2000). *The Fourier transform and its applications*. New York, NY: McGraw-Hill.

Bureau of Meteorology (2012). *Record-breaking La Niña events (Tech. Rep.)*. Canberra: Commonwealth of Australia. Retrieved from http://www.bom.gov.au/climate/enso/history/ln-2010-12/index.shtml

Chamberlin, P. C., Woods, T. N., Eparvier, F. G., & Jones, A. R. (2009). Next generation X-ray sensor (XRS) for the NOAA GOES-R satellite series. *Solar Physics and Space Weather Instrumentation III*, *7438*, 743–802. https://doi.org/10.1117/12.826807

Chapman, S. C., Lang, P. T., Dendy, R. O., Giannone, L., & Watkins, N. W. (2018). Control system-plasma synchronization and naturally occurring edge localized modes in a Tokamak. *Physics of Plasmas*, *25*, 062511. https://doi.org/10.1063/1.5025333

Chapman, S. C., Lang, P. T., Dendy, R. O., Watkins, N. W., Dunne, M., Giannone, L., et al. (2018). Intrinsic ELMing in ASDEX Upgrade and global control system-plasma self-entrainment. *Nuclear Fusion*, *58*, 126003. https://doi.org/10.1088/1741-4326/aadd1c

Chen, C.-C., McCarl, B. A., & Adams, R. M. (2001). Economic implications of potential ENSO frequency and strength shifts. *Climatic Change*, *49*, 147–159.

Chree, C. (1913). Some phenomena of sunspots and of terrestrial magnetism at Kew observatory. *Philosophical Transactions of the Royal Society of London, Series A*, *212*, 75–116. https://doi.org/10.1098/rsta.1913.0003

Deckert, R., & Dameris, M. (2008). From ocean to stratosphere. *Science*, *322*(5898), 53–55. https://doi.org/10.1126/science.1163709

Delaboudinière, J.-P., Artzner, G. E., Brunaud, J., Gabriel, A. H., Hochedez, J. F., Millier, F., et al. (1995). EIT: Extreme-ultraviolet imaging telescope for the SOHO mission. *Solar Physics*, *162*, 291–312. https://doi.org/10.1007/BF00733432

Deser, C., Phillips, A. S., & Hurrell, J. W., (2004). Pacific interdecadal climate variability: Linkages between the tropics and the North Pacific during Boreal Winter since 1900. *Journal of Climate*, *17*, 3109–3124. https://doi.org/10.1175/1520-0442(2004)017⟨3109:PICVLB⟩2.0.CO;2

Dikpati, M., McIntosh, S. W., Chatterjee, S., Banerjee, D., Yellin-Bergovoy, R., & Srivastava, A. (2019). Triggering the birth of new cycle's sunspots by solar tsunami. *Scientific Reports*, *9*, 2035. https://doi.org/10.1038/s41598-018-37939-z

Domeisen, D. I. V., Garfinkel, C. I., & Butler, A. H. (2019). The teleconnection of El Niño Southern Oscillation to the stratosphere. *Reviews of Geophysics*, *57*, 5–47. https://doi.org/10.1029/2018RG000596

Dunstone, N., Smith, D., Scaife, A., Hermanson, L., Eade, R., Robinson, N., et al. (2016). Skilful predictions of the winter North Atlantic Oscillation one year ahead. *Nature Geoscience*, *9*(11), 809–814. https://doi.org/10.1038/ngeo2824

Forbush, S. E. (1954). World-wide cosmic-ray variations, 1937–1952. *Journal of Geophysical Research*, *59*, 525–542. https://doi.org/10.1029/JZ059i004p00525

Gray, L. J., Beer, J., Geller, M., Haigh, J. D., Lockwood, M., Matthes, K., et al. (2010). Solar influences on climate. *Reviews of Geophysics*, *48*, RG4001. https://doi.org/10.1029/2009RG000282

Gutierrez, L. (2017). Impacts of El Niño-Southern Oscillation on the wheat market: A global dynamic analysis. *PLoS ONE*, *12*, e0179086. https://doi.org/10.1371/journal.pone.0179086

Harrison, R. G. (2004). The global atmospheric electrical circuit and climate. *Surveys in Geophysics*, *25*(5), 441–484. https://doi.org/10.1007/s10712-004-5439-8

Hathaway, D. H. (2015). The solar cycle. *Living Reviews in Solar Physics*, *12*, 4. https://doi.org/10.1007/lrsp-2015-4

Hurd, G. A., & Cameron, J. (1984). *The Terminator*. Los Angeles, CA: Orion.

Hurrell, J. W. (1995). Decadal trends in the North Atlantic Oscillation: Regional temperatures and precipitation. *Science*, *269*, 676–679. https://doi.org/10.1126/science.269.5224.676

Iizumi, T., Luo, J.-J., Challinor, A. J., Sakuari, G., Yokozawa, M., Sakuma, H., et al. (2014). Impacts of El Niño Southern Oscillation on the global yields of major crops. *Nature Communications*, *5*, 3712. https://doi.org/10.1038/ncomms4712

Kristjánsson, J. E., Staple, A., Kristiansen, J., & Kaas, E. (2002). A new look at possible connections between solar activity, clouds and climate. *Geophysical Research Letters*, *29*(23), 2107. https://doi.org/10.1029/2002GL015646

Leamon, R. J., McIntosh, S. W., Chapman, S. C., & Watkins, N. W. (2020). Timing terminators: Forecasting sunspot Cycle 25 onset. *Solar Physics*, *295*, 36. https://doi.org/10.1007/s11207-020-1595-3

Lemen, J. R., Title, A. M., Akin, D. J., Boerner, P. F., Chou, C., Drake, J. F., et al. (2012). The Atmospheric Imaging Assembly (AIA) on the Solar Dynamics Observatory (SDO). *Solar Physics*, *275*, 17–40. https://doi.org/10.1007/s11207-011-9776-8

Mantua, N. J., Hare, S. R., Zhang, Y., Wallace, J. M., & Francis, R. C. (1997). A Pacific interdecadal climate oscillation with impacts on salmon production. *Bulletin of the American Meteorological Society*, *78*(6), 1069–1079. https://doi.org/10.1175/1520-0477(1997)078%E81069:APICOW%E92.0.CO;2

McIntosh, S. W., Cramer, W. J., Pichardo Marcano, M., & Leamon, R. J. (2017). The detection of Rossby-like waves on the Sun. *Nature Astronomy*, *1*, 0086. https://doi.org/10.1038/s41550-017-0086

McIntosh, S. W., & Leamon, R. J. (2015). Deciphering solar magnetic activity: On grand minima in solar activity. *Frontiers in Astronomy and Space Sciences*, *2*, 2. https://doi.org/10.3389/fspas.2015.00002

McIntosh, S. W., & Leamon, R. J. (2017). Deciphering solar magnetic activity: Spotting solar cycle 25. *Frontiers in Astronomy and Space Sciences*, *4*, 4. https://doi.org/10.3389/fspas.2017.00004

McIntosh, S. W., Leamon, R. J., Egeland, R., Dikpati, M., Fan, Y., & Rempel, M. (2019). What the death of solar cycles imply about the nature of the solar interior. *Solar Physics*, *294*(7), 88. https://doi.org/10.1007/s11207-019-1474-y

McIntosh, S. W., Leamon, R. J., Gurman, J. B., Olive, J.-P., Cirtain, J. W., Hathaway, D. H., et al. (2013). Hemispheric asymmetries of solar photospheric magnetism: Radiative, particulate, and heliospheric impacts. *The Astrophysical Journal*, *765*, 146. https://doi.org/10.1088/0004-637X/765/2/146

McIntosh, S. W., Wang, X., Leamon, R. J., Davey, A. R., Howe, R., Krista, L. D., et al. (2014). Deciphering solar magnetic activity. I: On the relationship between the sunspot cycle and the evolution of small magnetic features. *The Astrophysical Journal*, *792*, 12. https://doi.org/10.1088/0004-637X/792/1/12

McPhaden, M. J. (2015). Playing hide and seek with El Niño. *Nature Climate Change*, *5*(9), 791–795. https://doi.org/10.1038/nclimate2775

Meehl, G. A., Arblaster, J. M., Matthes, K., Sassi, F., & van Loon, H. (2009). Amplifying the Pacific climate system response to a small 11-year solar cycle forcing. *Science*, *325*, 1114. https://doi.org/10.1126/science.1172872

Meyers, G., (1979). On the annual Rossby wave in the tropical North Pacific Ocean. *Journal of Physical Oceanography*, *9*, 663–674. https://doi.org/10.1175/1520-0485(1979)009<0663:OTARWI>2.0.CO;2

Morgan, H., & Taroyan, Y. (2017). Global conditions in the solar corona from 2010 to 2017. *Science Advances*, *3*, e1602056. https://doi.org/10.1126/sciadv.1602056

National Academies of Sciences, Engineering, and Medicine. (2016). *Next generation Earth system prediction: Strategies for subseasonal to seasonal forecasts*. Washington, DC: The National Academies Press. https://doi.org/10.17226/21873

Pierce, J. R. (2017). Cosmic rays, aerosols, clouds, and climate: Recent findings from the CLOUD experiment. *Journal of Geophysical Research: Atmospheres*, *122*, 8051–8055. https://doi.org/10.1002/2017JD027475

Pikovsky, A., Rosenblum, M., Kurths, J., & Hilborn, R. C. (2002). Synchronization: A universal concept in nonlinear science. *American Journal of Physics*, *70*(6), 655. https://doi.org/10.1119/1.1475332

Pinker, R. T., Grodsky, S. A., Zhang, B., Busalacchi, A., & Chen, W. (2017). ENSO impact on surface radiative fluxes as observed from space. *Journal of Geophysical Research: Oceans*, *122*, 7880–7896. https://doi.org/10.1002/2017JC012900

Prikryl, P., Muldrew, D. B., & Sofko, G. J. (2009). The influence of solar wind on extratropical cyclones—Part 2: A link mediated by auroral atmospheric gravity waves? *Annales Geophysicae*, *27*, 31–57. https://doi.org/10.5194/angeo-27-31-2009

Ramaswamy, V., Schwarzkopf, M. D., Randel, W. J., Santer, B. D., Soden, B. J., & Stenchikov, G. L. (2006). Anthropogenic and natural influences in the evolution of lower stratospheric cooling. *Science*, *311*(5764), 1138–1141. https://doi.org/10.1126/science.1122587

Roberts, W. O., & Olson, R. H., (1973, January). Geomagnetic storms and wintertime 300-mb trough development in the North Pacific-North America Area. *Journal of the Atmospheric Sciences*, *30*, 135–140. https://doi.org/10.1175/1520-0469(1973)030<0135:GSAWMT>2.0.CO;2

Rosenlof, K. H., & Reid, G. C. (2008). Trends in the temperature and water vapor content of the tropical lower stratosphere: Sea surface connection. *Journal of Geophysical Research*, *113*, D06107. https://doi.org/10.1029/2007JD009109

Rybansky, M., Rusin, V., Minarovjech, M., & Gaspar, P. (1994). Coronal index of solar activity: Years 1939–1963. *Solar Physics*, *152*, 153–159. https://doi.org/10.1007/BF01473198

Saba, J. L. R., Strong, K. T., & Slater, G. L. (2005). Can we predict when the next solar cycle is about to take off? *Memorie della Societa Astronomica Italiana*, *76*, 1034.

Scherrer, P. H., Wilcox, J. M., Svalgaard, L., Duvall, T. L., Jr., Dittmer, P. H., & Gustafson, E. K. (1977). The mean magnetic field of the sun—Observations at Stanford. *Solar Physics*, *54*, 353–361. https://doi.org/10.1007/BF00159925

Schonfeld, S. J., White, S. M., Hock-Mysliwiec, R. A., & McAteer, R. T. J. (2017). The slowly varying corona. I: Daily differential emission measure distributions derived from EVE spectra. *The Astrophysical Journal*, *844*, 163. https://doi.org/10.3847/1538-4357/aa7b35

SILSO World Data Center. (1960–2020). *The International sunspot number. International sunspot number monthly Bulletin and online catalog*.

Smith, D. M., Scaife, A. A., Eade, R., & Knight, J. R. (2016). Seasonal to decadal prediction of the winter north atlantic oscillation: Emerging capability and future prospects. *Quarterly Journal of the Royal Meteorological Society*, *142*, 611–617. https://doi.org/10.1002/qj.2479

Snow, M., Weber, M., Machol, J., Viereck, R., & Richard, E. (2014). Comparison of Magnesium ii core-to-wing ratio observations during solar minimum 23/24. *Journal of Space Weather and Space Climate*, *4*, A04. https://doi.org/10.1051/swsc/2014001

Strong, K. T., & Saba, J. L. R. (2009). A new approach to solar cycle forecasting. *Advances in Space Research*, *43*, 756–759. https://doi.org/10.1016/j.asr.2008.12.007

Svensmark, H., & Friis-Christensen, E. (1997). Variation of cosmic ray flux and global cloud coverage–a missing link in solar-climate relationships. *Journal of Atmospheric and Solar-Terrestrial Physics*, *59*, 1225–1232. https://doi.org/10.1016/S1364-6826(97)00001-1

Svensmark, J., Enghoff, M. B., Shaviv, N. J., & Svensmark, H. (2017). Increased ionization supports growth of aerosols into cloud condensation nuclei. *Nature Communications*, *8*, 2199. https://doi.org/10.1038/s41467-017-02082-2

Tapping, K. F. (2013). The 10.7 cm solar radio flux ($F_{10.7}$). *Space Weather*, *11*, 394–406. https://doi.org/10.1002/swe.20064

Teisberg, T. J. (1999). *Effects of 1997–1998 El Niño on natural gas and distillate fuel oil costs*. Washington, DC: U.S. Department of Commerce, National Oceanic and Atmospheric Administration.

Thompson, D. W. J., & Solomon, S. (2005). Recent stratospheric climate trends as evidenced in radiosonde data: Global structure and tropospheric linkages. *Journal of Climate*, *18*, 4785–4795. https://doi.org/10.1175/JCLI3585.1

Tinsley, B. A. (2000). Influence of solar wind on the global electric circuit, and inferred effects on cloud microphysics, temperature, and dynamics in the troposphere. *Space Science Reviews*, *94*, 231–258.

Tinsley, B. A., Brown, G. M., & Scherrer, P. H. (1989). Solar variability influences on weather and climate: Possible connections through cosmic ray fluxes and storm intensification. *Journal of Geophysical Research*, *94*, 14783–14792. https://doi.org/10.1029/JD094iD12p14783

Trenberth, K. E, & Stepaniak, D. P., (2001). Indices of El Niño evolution. *Journal of Climate*, *14*, 1697–1701. https://doi.org/10.1175/1520-0442(2001)014⟨1697:LIOENO⟩2.0.CO;2

van Loon, H., Meehl, G. A., & Arblaster, J. M. (2004). A decadal solar effect in the tropics in July-August. *Journal of Atmospheric and Solar-Terrestrial Physics*, *66*, 1767–1778. https://doi.org/10.1016/j.jastp.2004.06.003

Vecchi, G. A., & Soden, B. J. (2007a). Global warming and the weakening of the tropical circulation. *Journal of Climate*, *20*, 4316. https://doi.org/10.1175/JCLI4258.1

Vecchi, G. A., & Soden, B. J. (2007b). Increased tropical Atlantic wind shear in model projections of global warming. *Geophysical Research Letters*, *34*, L08702. https://doi.org/10.1029/2006GL028905

Weiher, R. F. (Ed.) (1999). *Improving El Niño forecasting: The potential economic benefits*. Washington, DC: U.S. Department of Commerce, National Oceanic and Atmospheric Administration.

Weiher, R. F., & Kite-Powell, H. L. (1999). *Assessing the economic impacts of El Niño and benefits of improved forecasts*. Washington, DC: U.S. Department of Commerce, National Oceanic and Atmospheric Administration.

White, W. B., & Liu, Z. (2006). Resonant excitation of the quasidecadal oscillation by the 11year signal in the Sun's irradiance. *Journal of Geophysical Research*, *113*, C01002. https://doi.org/10.1029/2006JC004057

Wilcox, J. M., Hoeksema, J. T., & Scherrer, P. H. (1980). Origin of the warped heliospheric current sheet. *Science*, *209*, 603–605. https://doi.org/10.1126/science.209.4456.603

Wilson, P. R., Altrock, R. C., Harvey, K. L., Martin, S. F., & Snodgrass, H. B. (1988). The extended solar activity cycle. *Nature*, *333*, 748–750. https://doi.org/10.1038/333748a0

Woods, T. N., Eparvier, F. G., Hock, R., Jones, A. R., Woodraska, D., Judge, D., et al. (2012). Extreme Ultraviolet Variability Experiment (EVE) on the Solar Dynamics Observatory (SDO): Overview of science objectives, instrument design, data products, and model developments. *Solar Physics*, *275*, 115–143. https://doi.org/10.1007/s11207-009-9487-6

Zhou, C., Zelinka, M. D., & Klein, S. A. (2016). Impact of decadal cloud variations on the Earth's energy budget. *Nature Geoscience*, *9*, 871–874. https://doi.org/10.1038/ngeo2828